DOI: https://doi.org/10.71317/kjard.2.11.2026.1078

Kashmir Journal of Academic Research and Development

Journal homepage: https://rjsaonline.org/index.php/KJARD

Green Synthesis of Biopolymer-Based Nanocomposite for Environmental Applications

Muhammad Rashid Naveed
University of Education Lahore, Multan Campus, Pakistan
Email: msf2206174@ue.edu.pk
Samavia Batool
Department of Environmental Science, PMAS Arid Agriculture University, Rawalpindi, Pakistan
Email: samaviab@yahoo.com
Awais Zakeer
Advanced Membrane Technology Research Centre (AMTEC), Faculty of Chemical and Energy Engineering, University Technology Malaysia, Johor, Malaysia
Email: awaiszakeer@gmail.com
Nasreen Ashraf
Department of Chemistry, Government Girls Degree College No. 1 Dera Ismail Khan (Affiliated with Gomal University), KPK, Pakistan
Email: nasreenashraf.714@gmail.com
Rabail Urooj
Department of Environmental Sciences, Sardar Bahadur Khan Women's University, Quetta, Pakistan
Email: rabailurooj@gmail.com
Waqas Ahmad
Specialized Healthcare & Medical Education Department, (SHC&MED) Services Institute of Medical Sciences (SIMS) /Services Hospital, Lahore
Email: drwaqasahmadrajpoot@gmail.com

ARTICLE INFO

Received:
October 16, 2026
Revised:
October 31, 2026
Accepted:
November 09, 2026
Available Online:
November 19, 2026

Keywords:
Blood transfusion, registered nurses, knowledge, clinical practices, transfusion safety, transfusion reactions, patient safety.

Corresponding Author:
Nasreen Ashraf, Waqas Ahmad
Email:
nasreenashraf.714@gmail.com, drwaqasahmadrajpoot@gmail.com

ABSTRACT

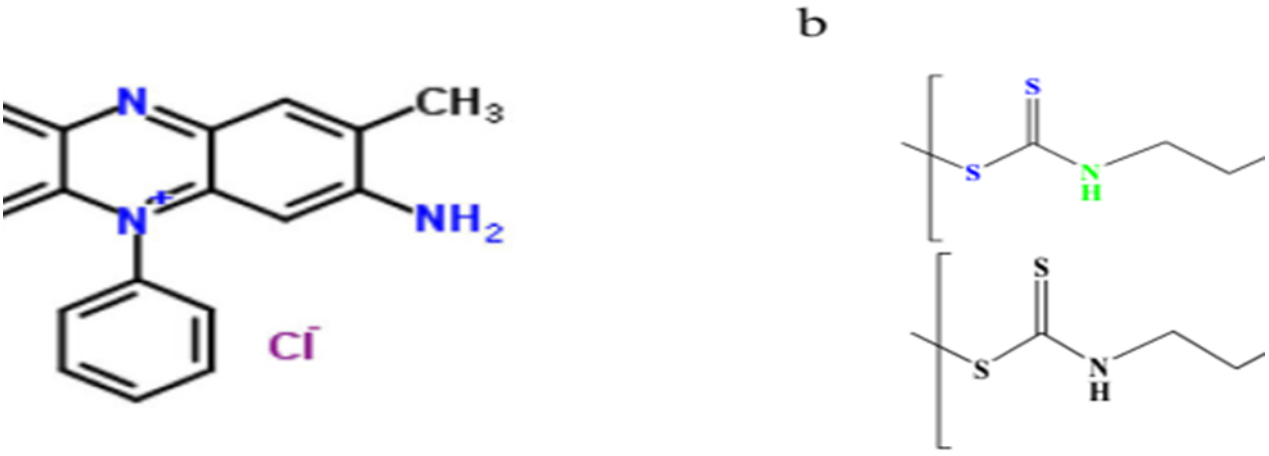
Industrial and agricultural activities release dyes and pesticides into aquatic environments, creating risks for ecosystems and human health. This study investigated a maize-biochar/zinc oxide nanocomposite (MB-ZnO), prepared by solvent-free ball milling, as a material for removing Safranin O (Saf) and Mancozeb (MC) from aqueous solutions. We pyrolyzed maize straw at 600 °C to produce biochar, then combined it with ZnO and milled it. We characterized the resulting composite using scanning electron microscopy (SEM), energy-dispersive X-ray spectroscopy (EDX), X-ray diffraction (XRD), Fourier-transform infrared spectroscopy (FTIR), thermogravimetric analysis (TGA), and UV–Vis spectroscopy. Adsorption and pollutant removal were evaluated under dark, ultraviolet (UV), and visible-light conditions. The composite removed Safranin O by 83.5% under visible light, 81.0% under UV light, and 78.0% in the dark within 60 min. For Mancozeb, removal reached 56.5% under visible light and 27.5% under UV light; removal in the dark was 25.2%. The enhanced removal under visible light suggests that combining maize biochar with ZnO may improve pollutant removal through complementary adsorption and light-assisted processes. The use of an agricultural waste-derived material and a solvent-free synthesis approach offers a potentially sustainable strategy for developing cost-effective materials for water treatment. The results indicate that MB-ZnO can remove both target pollutants under the tested conditions, with the strongest performance generally observed under visible light. Further work should distinguish adsorption from chemical degradation and verify performance in more complex wastewater matrices.

Introduction

Industrial development has improved production and daily life, but it has also increased the release of contaminants into the environment. Industrial effluents may contain synthetic dyes and metals, while agricultural runoff can carry pesticides and their transformation products into soils and water. Dyes from textile, paper, leather, cosmetic, and related industries can reduce light penetration in water and interfere with aquatic photosynthesis. Pesticides are widely used to protect crops and control pests; however, their residues may reach surrounding ecosystems through runoff and leaching . These concerns have prompted the development of treatment approaches that are effective, affordable, and environmentally responsible. Existing methods include ozonation, coagulation, advanced oxidation, biological degradation, and ion exchange, although their cost and operational requirements can limit their application. Photocatalysis is one potential approach for removing contaminants from water.

Biochar, a carbon-rich material produced by heating biomass under oxygen-limited conditions, has attracted interest as an adsorbent and catalyst support. Agricultural residues, including straw, are abundant feedstocks for biochar production. The porous structure created during pyrolysis can provide sites for contaminant adsorption. Combining biochar with metal oxides is one strategy for developing materials that integrate adsorption with photocatalytic activity. In particular, solvent-free ball milling is a relatively simple approach for combining materials, reducing particle size, and modifying surface properties without requiring a liquid solvent. Zinc oxide (ZnO) is a semiconductor photocatalyst, while biochar can provide a high-surface-area support and may facilitate interactions between the pollutant, carbon surface, and ZnO particles. The performance of such composites depends on their preparation, structure, and operating conditions and therefore requires experimental evaluation. Plant-derived cellulose nanofibers have also been investigated as bio-based adsorbents for removing aqueous contaminants.

Safranin O (also known as Basic Red 2) is a cationic dye used in applications such as textile and paper staining, paints, and printing inks. Its release into wastewater can create environmental concerns.. Mancozeb is a widely used fungicide, including in the production of tomato, potato, and fruit crops. This study evaluated a maize-biochar/ZnO composite prepared by solvent-free ball milling for the removal of Safranin O and Mancozeb from aqueous solutions under dark, UV, and visible-light conditions. The work examined the composite's physicochemical properties and compared pollutant removal under the different conditions. The results are intended to assess the potential of the material for further investigation in water-treatment applications; they do not, by themselves, establish its suitability for full-scale treatment.



Materials and methods

Plant material

Maize straw was collected from farmland in the Islamabad Capital Territory, Pakistan, and crushed to a particle size of 1–1.5 mm for biochar preparation. Safranin O, Mancozeb, ZnO, NaOH, and HCl were purchased commercially. Deionized water was used to prepare the solutions.

Synthesis of biochar

Maize biochar (MB) was prepared following a previously reported protocol. Briefly, maize straw was cut into pieces, washed with deionized water, shade-dried, crushed, and sieved. A 10 g portion of the sieved material was placed in a crucible and pyrolyzed in a vacuum furnace at 600 °C for 6 h. The resulting biochar was passed through an 80-mesh sieve and stored until use.

Synthesis of nanocomposite

The MB-ZnO nanocomposite was prepared by mixing maize biochar and zinc oxide at a 50:50 mass ratio. Approximately 6 g of the mixture was transferred to a 500 mL agate jar containing 180 g of 6 mm agate balls. The ball-to-powder mass ratio was 15:1. The mixture was milled in a horizontal oscillatory planetary mill for 72 h under ambient conditions. The milled material was used directly without adding a liquid solvent.

Characterization of MB-ZnO nanocomposite

The morphology of the nanocomposite was examined by scanning electron microscopy (SEM; JEOL JSM 25910). Crystalline structure was analyzed by X-ray diffraction (XRD; Bruker D8) over a 2θ range of 0–80°. Thermal behavior was assessed using a thermogravimetric analyzer (METTLER TOLEDO TGA/SDTA 851). Elemental composition was analyzed by energy-dispersive X-ray spectroscopy (EDX; UKINCA 200), and functional groups were examined by Fourier-transform infrared spectroscopy (FTIR; SPECTRUM 65). Optical properties were assessed by UV–Vis diffuse-reflectance spectroscopy over 200–800 nm. Band-gap energies were estimated from the optical data.

Adsorption and photocatalysis performances against organic and inorganic pollutants

Stock solutions of pollutants

To evaluate adsorption and pollutant removal under different illumination conditions, separate stock solutions of Safranin O (Saf) and Mancozeb (MC) were prepared. For Saf, 15 mg was dissolved in 300 mL of water. The solution was divided equally among three flasks, each containing 100 mL, and 5 mg of MB-ZnO was added to each flask. The pH was measured and adjusted to 6.8. The Mancozeb solution was prepared using the same stated concentrations and procedure.

Adsorption experiments in dark conditions

Dark-condition adsorption tests for Saf and MC were performed separately at 25 °C. For the Saf test, the suspension in a 100 mL flask was sonicated for 1 h to obtain a uniform mixture and then stirred. At 10 min intervals, 3 mL samples were collected, centrifuged at 4000 rpm for 5 min, and passed through a 0.45 μm syringe filter. Saf concentration was measured using a UV–Vis spectrophotometer (Evolution 300) at 660 nm. The same sampling and analysis procedure was used for MC.

Photocatalysis experiment

Photocatalytic removal of Saf and MC was assessed under visible and UV light. Based on a previously reported procedure, the MB-ZnO dose was 5 mg per 100 mL of solution. For each pollutant, two 100 mL flasks were sonicated for 1 h to disperse the material. One flask was exposed to visible light from a 500 W xenon lamp, while the other was placed in a separate closed container under a 400 W UV source. The lamps were positioned approximately 10 cm above the solutions, which were stirred for 60 min. Temperature and pH were maintained at approximately 25 °C and 6.8, respectively. Samples of 3 mL were collected every 10 min, centrifuged at 4000 rpm for 5 min, and filtered through a 0.45 μm syringe filter. Pollutant concentrations were measured by UV–Vis spectrophotometry at 660 nm for Saf; the same procedure was reported for MC.

lated with a UV–Vis spectrophotometer at 660 nm wavelength. The same procedure was followed for the estimation of MC. The degradation percentage rate of both Saf and MZ via MB-ZnO nanocomposite was calculated by the following formula:

g ¼ Co Ct=Co 100 2Þ

where g (%) indicates the degradation percentage of pollu- tants. Co and Ct(mg/L) stand for the primary concentration and equilibrium concentration of pollutants respectively. The photocatalytic activities of prepared biochar nano- composites were measured by studying the discoloration of Saf and MC solutions.

Total organic carbon analysis (TOC)

Total organic carbon (TOC) was measured according to a previously reported method. Briefly, 1 mL of HCl was added to each sample, which was then diluted tenfold to remove carbonates and dissolved CO_2. TOC was measured using a total-organic-

carbon analyzer with an infrared detector. The temperature in the catalytic furnace was gradually raised to 700 °C to convert intermediate products to CO_2.

Kinetic study

Pollutant removal during irradiation was analyzed using the pseudo-first-order model within the Langmuir–Hinshelwood framework. The apparent rate constant was estimated from the slope of the linear relationship between $\ln(C_0/Ct)$ and time (min). Here, C_0 is the initial pollutant concentration, Ct is the concentration at time t, and kapp is the apparent rate constant. This model was used to compare the observed removal profiles under the tested light conditions.

ln Co=Ct Þ ¼ Kappt 3Þ

Initial decolorization rate constants were calculated from the slope of ln(Ct/Co) vs t (min.) plots. Where, Ct is the con- centration of pollutants (Saf and MC) at any given time, Co is the concentration of a pollutant at zero-time, t is the irradi- ation time and Kapp is the apparent kinetic constant. The whole light-driven degradation rate of Saf and MC by the photocatalyst followed pseudo-first-order kinetics.

Results and discussions

SEM and EDX analysis

The influence of ZnO on the biochar textural characteristics was examined by SEM analysis. SEM image revealed the por- ous and rough structure of pristine biochar (Fig. 2a). The por- ous and rough structure of MB is due to the removal of volatile substances during pyrolysis. These structural proper- ties of MB prove its ability to adsorb and support nano- sized particles. The SEM of MB-ZnO nanocomposite exhibited ultrafine white particulates of ZnO, in the form of clusters on the whole biochar surface (Fig. 2b). EDX micro analysis of MB-ZnO nanocomposite showed the existence of C, O, Ca, Si, K, Mg, Na, P, and Zn elements (Fig. 3a). Additionally, a strong peak of Zn in the EDX spectrum indicated the success- ful interpretation of ZnO by the Ball-milling process. The results obtained from characterization MB-ZnO nanocompos- ite undoubtedly confirm the presence of ZnO on the porous structure of biochar skeleton using ball milling to synthesize biochar/ZnO nanocomposites, which shows similar results to the published results of biochar nanocomposites from Bamboo stakes[37]. The results were further confirmed by the elemental analysis (Fig.

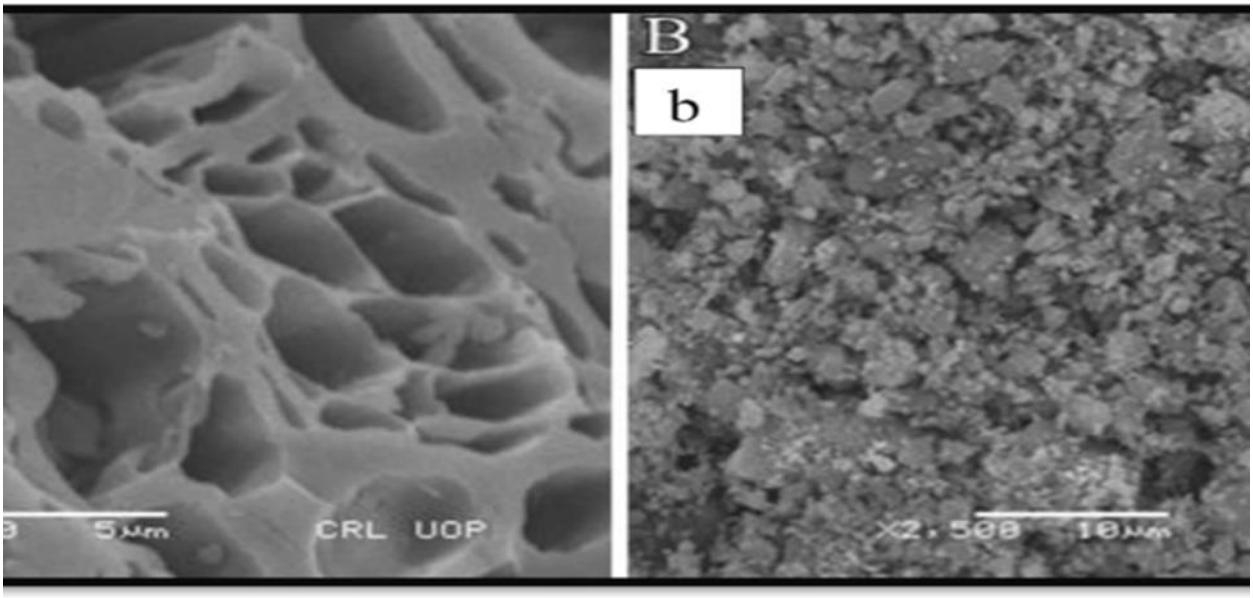
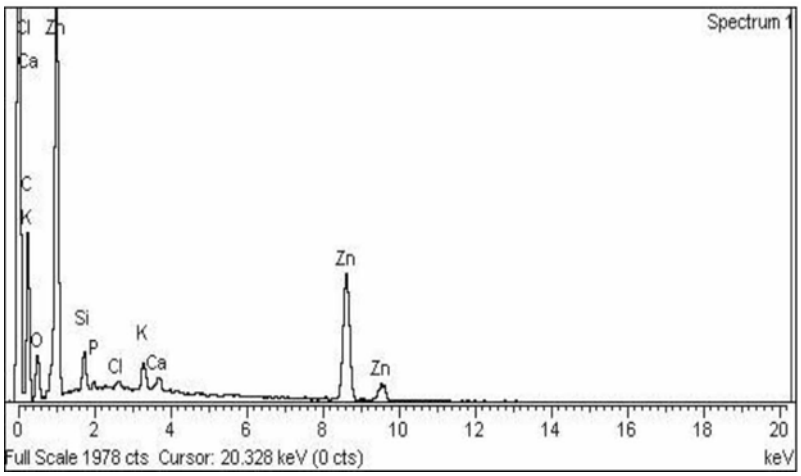


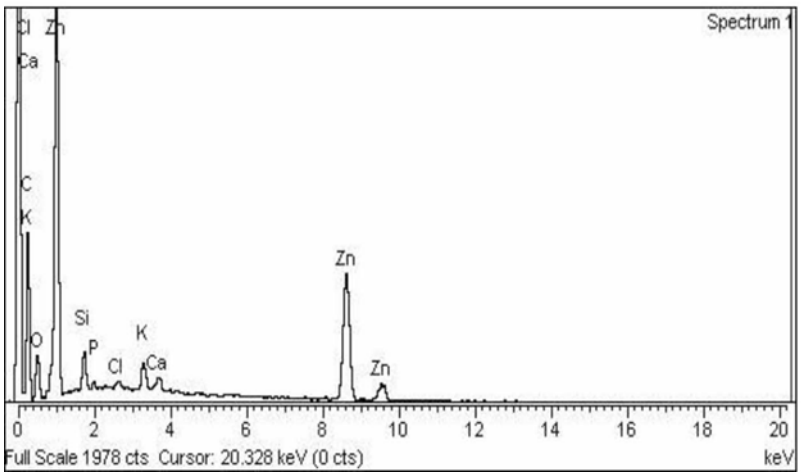
Fig. 2 SEM images of pure biochar (a) and MB-ZnO nanocomposite (b).

(a) **(b)**



Element	Weight%	Atomic%
C K	46.51	74.29
O K	9.17	11.00
Si K	2.22	1.52
P K	0.22	0.14
Cl K	0.54	0.29
K K	2.06	1.01
Ca K	1.21	0.58
Zn L	38.07	11.18
Totals	100.00	

(a) **(b)**



Element	Weight%	Atomic%
C K	46.51	74.29
O K	9.17	11.00
Si K	2.22	1.52
P K	0.22	0.14
Cl K	0.54	0.29
K K	2.06	1.01
Ca K	1.21	0.58
Zn L	38.07	11.18
Totals	100.00	

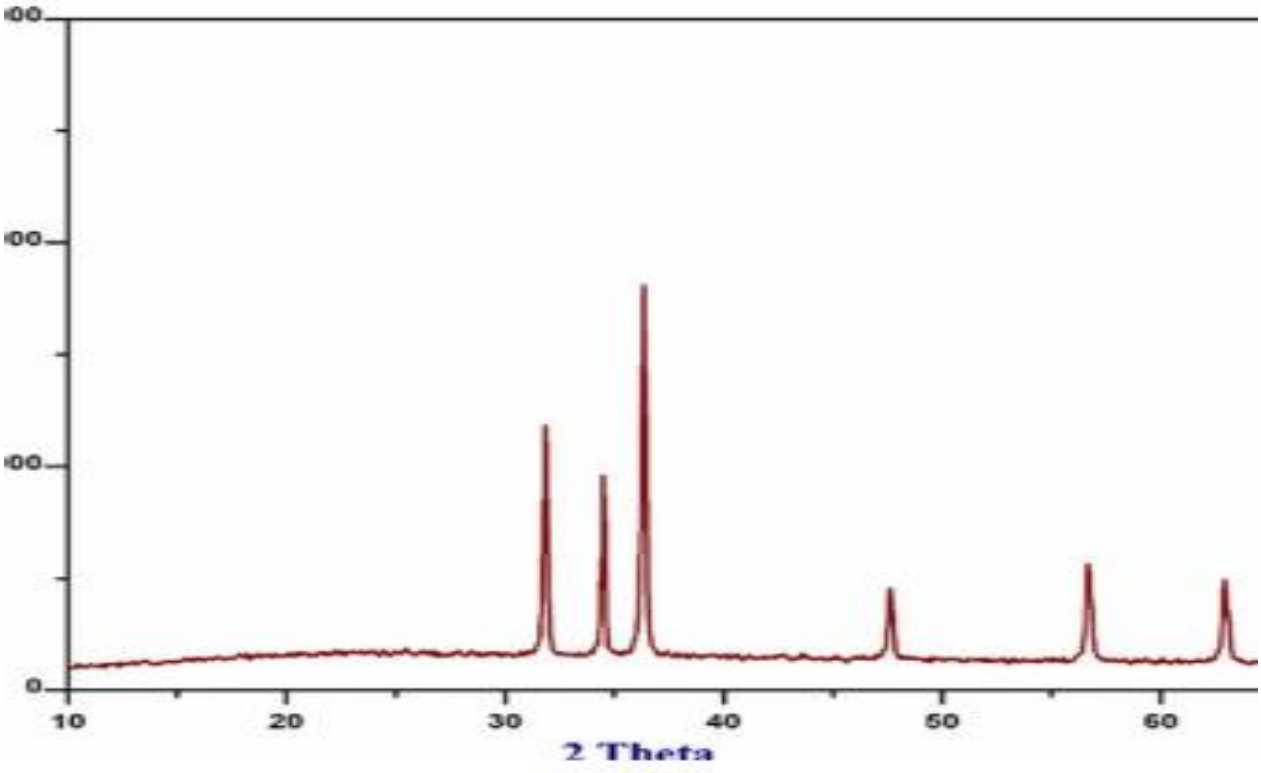


Fig. 4. XRD patterns of MB-ZnO nanocomposite.

FTIR analysis

FTIR analysis successfully determined various dominant functional groups of the nanocomposite (Fig. 5). In the FTIR analysis, nine different peaks were observed in the range of 500– 4000 cm1. The peaks observed at 520 cm1 and 556 cm1 rec- ognized the bending vibration of C-I stretching and C-Br stretching, respectively. The peaks located at 799 cm1 represented medium C = C bending of alkene. Similarly, the peaks at 1091 cm1 and 1571 cm1 indicated the strong stretching of C-O and medium stretching of C = C. The appearance of a broad peak at 3244 cm1 showed the strong and broad O–H stretching of alkyne. Interestingly, the high peak observed at 520 cm1 in the FTIR spectra is aligned with the previous results. An additional peak at 556 cm1 was observed in MB- ZnO nanocomposite, which indicated the presence of ZnO on the surface of MB**.**

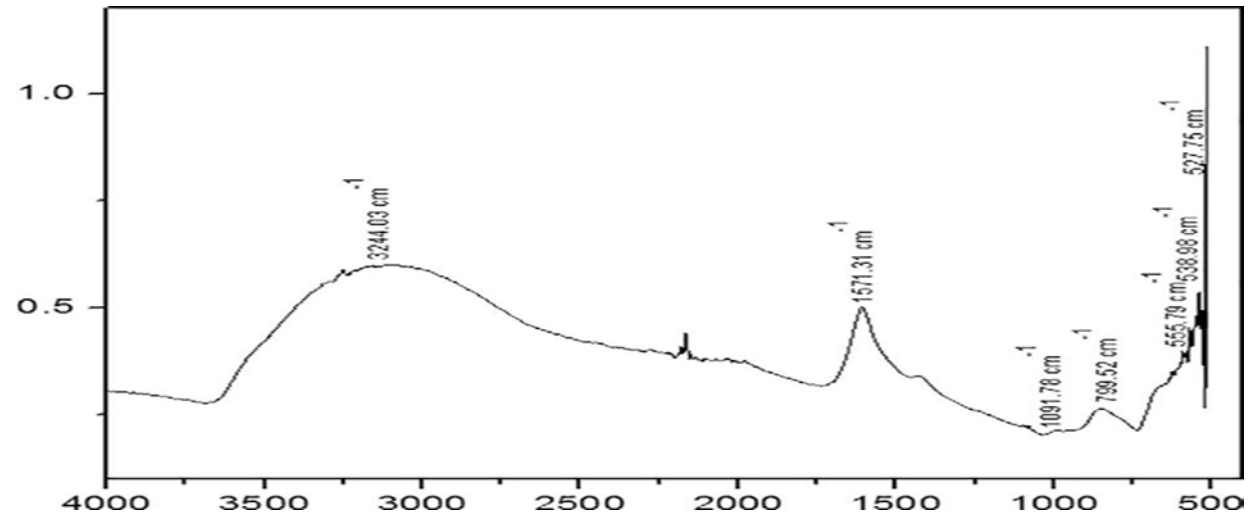


Fig. 5 FTIR analysis of MB-ZnO nanocomposite.

Thermogravimetric analysis (TGA)

TGA was performed to explore thermal properties and ranges where biomass devolatilization of various contents like water vapors and other impurities present in the sample occurs. TGA revealed the reduction in mass with increasing temperature. The initial loss of weight at low temperature corresponds to the evaporation of water molecules retained in the pores and particles' surfaces. This curve was formed due to a loss of 5% weight by the evaporation of water (50–100 C), further 5–8% weight loss by volatilization of hemicelluloses (150 C–350 C), another 10–12% loss by cellulose (300 C and 500 C), and another 20–25% loss by lignin (700 °C). Compared to the pristine biochar (Fig. 6a), the MB-ZnO nanocomposite (Fig. 6b) degraded slightly earlier. This indicates slightly lower thermal stability of the MB-ZnO nanocomposite than pristine biochar. Usually, pristine biochar has lower stability than the biochar- nanocomposite, but here biochar was prepared at a high temperature (600 °C), which might have improved the thermal properties of the pristine biochar. These results revealed good thermal stability of both pristine biochar and MB-ZnO nanocomposite.

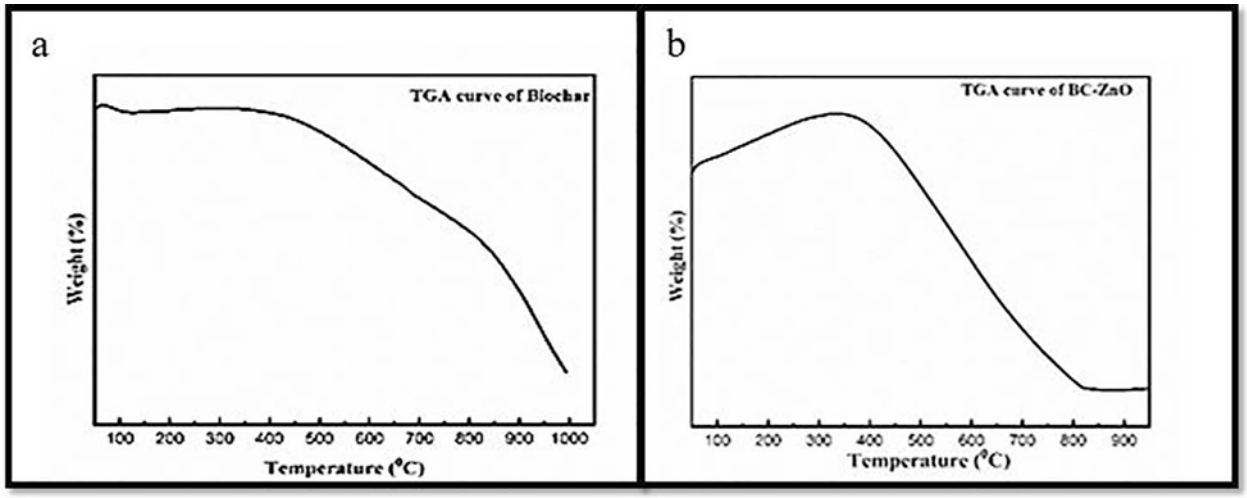


Fig. 6 Thermogravimetric analysis of pristine biochar (a) and MB-ZnO nanocomposites (b).

Optical properties analysis

For the determination and comparison of optical behavior, a small quantity of each sample (MB, ZnO, and MB-ZnO) was dispersed in deionized water under ultrasound irradiation for 5 min, and then the absorption spectrum was observed by a UV–Vis spectrometer. MB revealed a peak at 450 nm (Fig. 7a), while the peaks of ZnO and MB-ZnO nanocomposite were observed at 350 and 400 nm, respectively (Fig. 7b). The results of the absorption spectra are also a practical tool for bandgap determination. From the UV–Vis spectra, the values of bandgap energy were calculated. It is documented in the published research that the average band gap value for ZnO nanoparticles and BC- ZnO nanocomposite is 3.04 and 2.77 eV, respectively. The prepared composite showed band gap values of nearly 1.71 eV, which shows better results than those already reported. The process was carried on by applying the Tauc Plot method which is pulling extrapolation at the linear area from hv and (ahv)2 correlation graph up to its cut energy axis as shown in Fig. 7. Fig. 8 illustrates the relationship between bandgap energy (hv) and the coefficient it was absorbed in photon (ah)2 as the ordinate till it cut energy axis, and thus the bandgap energy value can be achieved. The reduction of bandgap in MB-ZnO may be due to the development of new energy states in the MB-ZnO nanocomposite brought by the interaction of MB and ZnO in the nanocomposite or may be due to some substances narrowing the band gap present in the prepared biomass carbon, which decreased the energy required for the electrons of ZnO to transition from the valence band to the conduction band. Several studies have documented that the loading of semiconductors like ZnO on non-metallic atoms (such as carbon, nitrogen, and Sulphur) can enhance their photocatalytic efficiency, because of the reduction of the bandgap and increase of the absorption range to the visible region. Moreover, it also increases electron/hole separation because of the tremendous double conductivity between carbonaceous materials and ZnO. Different factors that can cause the reduction of the bandgap were explained in detail in the synthesis of biochar-nanocomposite.

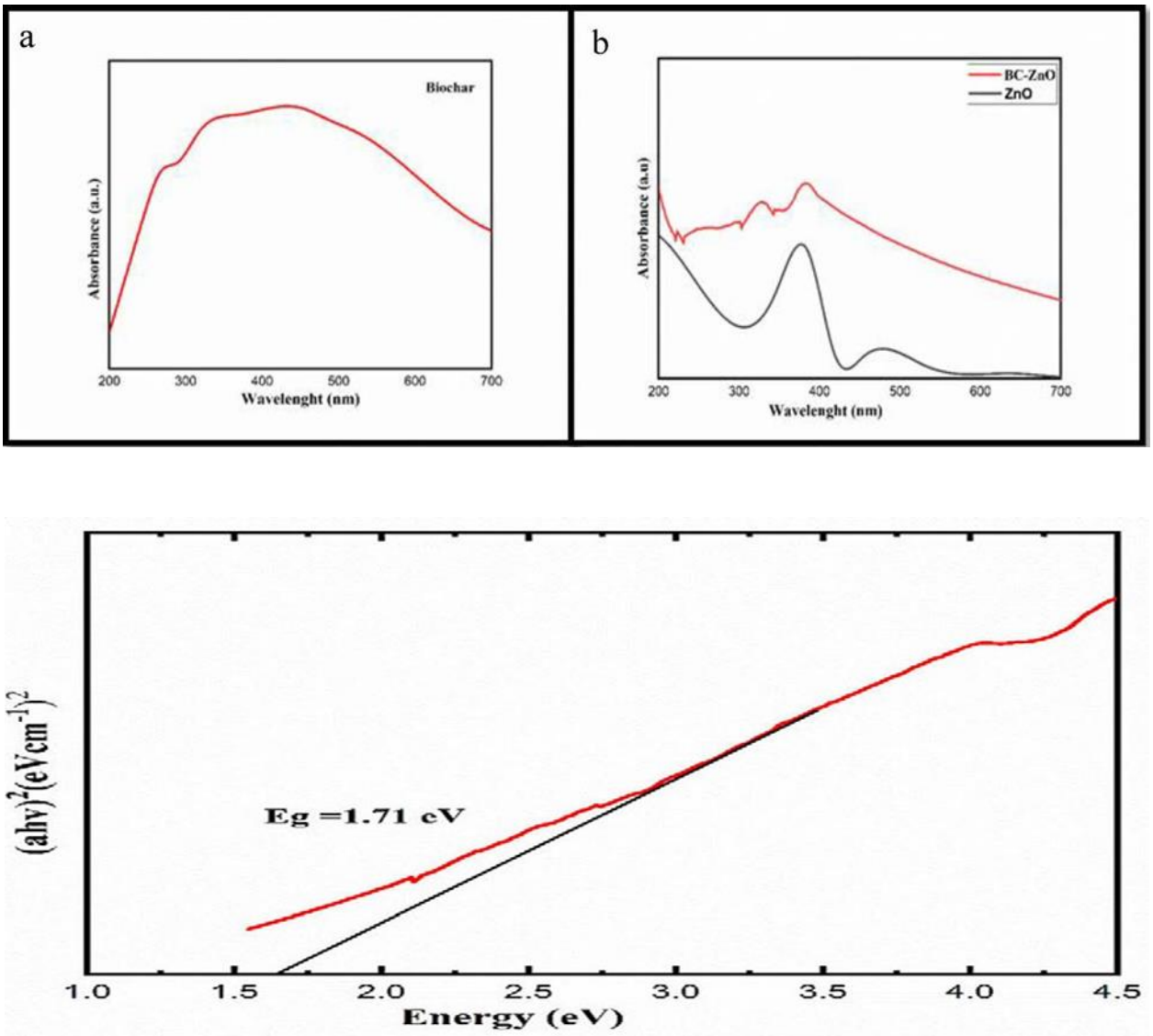


Fig. 8. Bandgap analysis of MB-ZnO nanocomposite.

Removal of Saf and MC using ZnO-biochar composite

The adsorption and photocatalytic activity of MB-ZnO nanocomposite was assessed in different light conditions by observing the removal of Saf and MC from aqueous solutions. All the MB-ZnO nanocomposite samples revealed good degra- dation of Saf in the dark and various light sources (Fig. 9). Application of MB-ZnO nanocomposite into the tubes suc- cessfully removed Saf by changing the color of the solution from pink is caused by the SF to transparent in an aqueous solution. A comparison of Safranin and Fungicide degradation efficiencies achieved in the current work and by different composites documented in the literature has been described in Table 1. All the MB-ZnO nanocomposite samples revealed good degradation of MC under the dark and various light sources (Fig. 10). A pure solution was achieved after adding MB-ZnO nanocomposite into the beaker, which showed the successful removal of MC by the nanocomposite. From the above results, it was concluded that MB-ZnO nanocomposite has better degradation efficiency against Saf than MC. It is most important that solvent-free ball-milled BC-ZnO showed good photodegradation of pollutants in the presence of visible light, possibly because of its good photocatalytic activity or the activation of its persistent free radicals by UV.

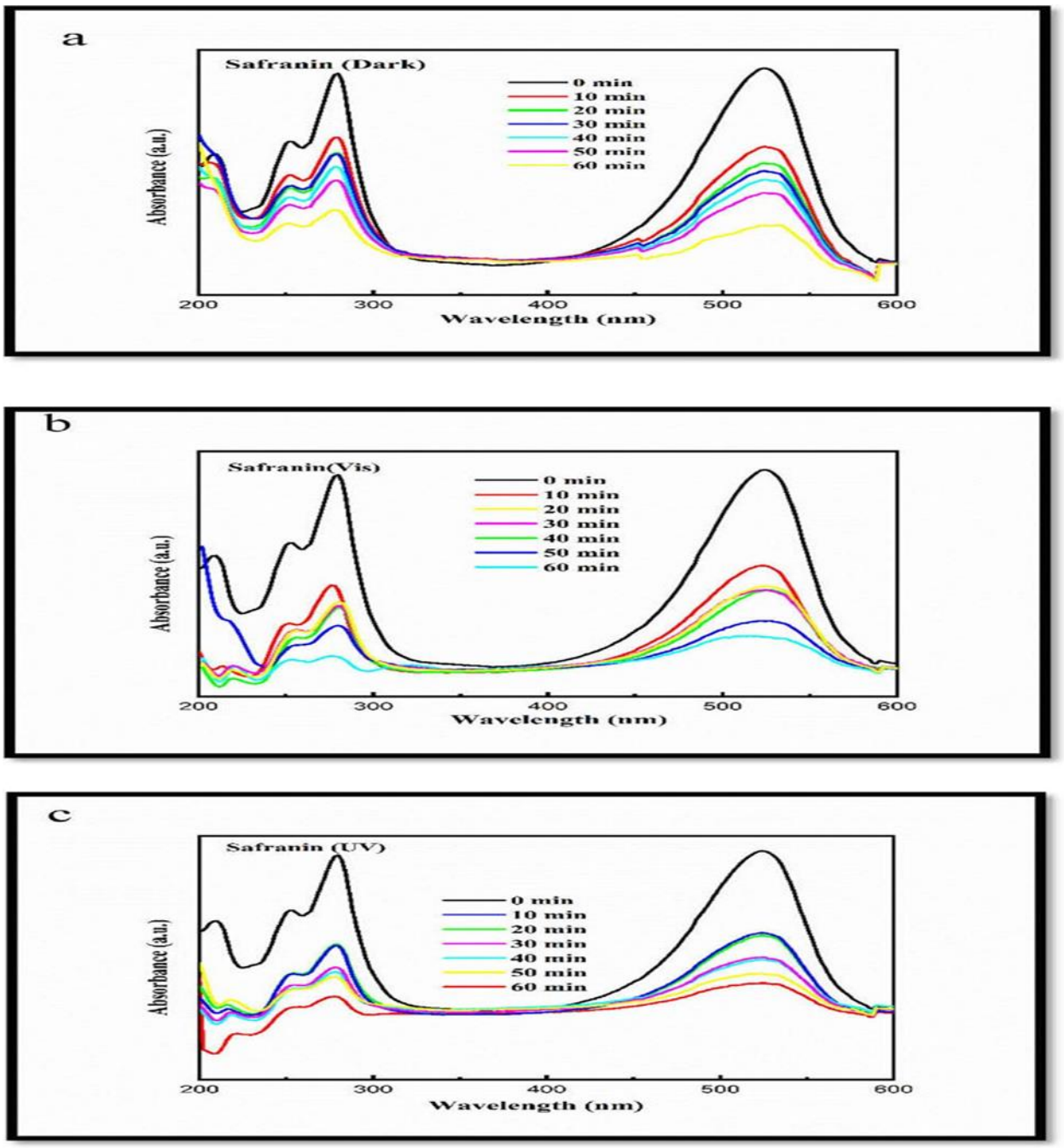


Fig. 9. Plot of Safranin degradation at different time intervals under dark (a), UV radiation (b), and visible light (c) conditions.

Table 1. Comparison of Safranin and fungicide degradation efficiencies reported in the literature and in the present study.

Contaminant	Reference	Material Conditions	Efficiency/time
Imidacloprid	[56]	C–ZnO	100 mg/L; catalyst dosage 100 mg/L; UV lamp	82% / 20 min
Diazinon	[57]	C–ZnO	10 mg/L; catalyst dosage 15 mg/L; UV lamp	58% / 30 min

Safranin	[58]	CuN NPs 20 mg/L; catalyst dosage 10 mg/L; UV lamp	95% / 70 min
Safranin	[59]	GS/ZnO 2.2×10^{-4} M; catalyst dosage 20 mg/L; visible light	20% / 60 min
Safranin	[60]	WO_3 200 mg/L; catalyst dosage 100 mg/L; laser	94% / 30 min
Safranin	Present study	MB/ZnO 15 mg/L; catalyst dosage 5 mg/L; visible light	87% / 60 min
Mancozeb	Present study	MB/ZnO 15 mg/L; catalyst dosage 5 mg/L; visible light	57% / 50 min

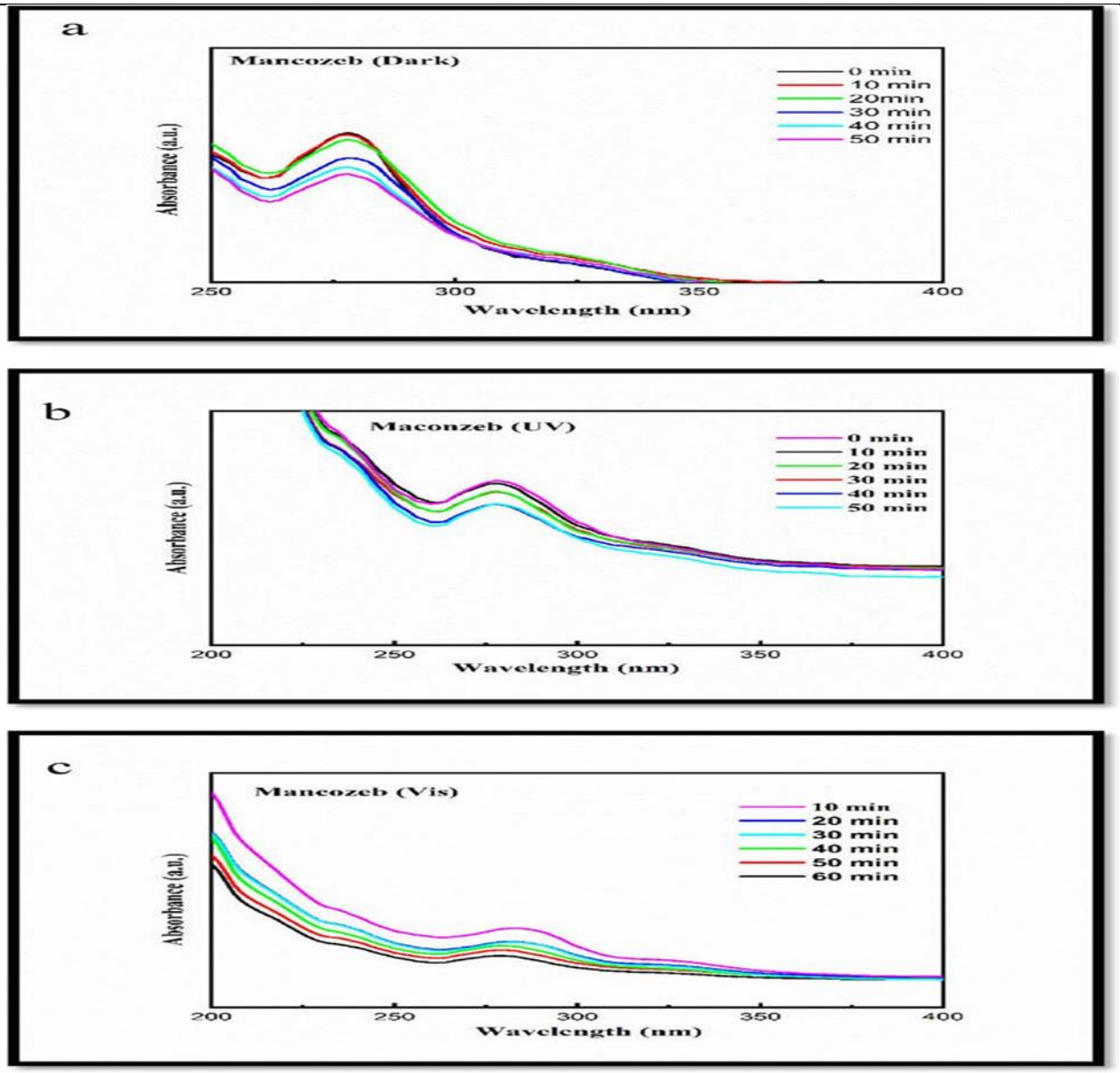


Fig. 10. Plot of MC degradation at different time intervals under dark (a), UV radiation (b), and visible light (c) conditions.

Degradation rate of pollutants

A sequence of experiments was performed to assess the photocatalytic performance of the MB-ZnO nanocomposites under dark, UV, and visible light sources at various irradiation times (0–60 min). The absorbance curves revealed the reduction of Safranin concentration over time under dark, UV, and Visible light conditions (Fig. 11a). The Safranin degradation showed steeper curves under visible and UV light than under dark conditions. The graph showed that the irradiation was performed at various rates in different media, but the removal of Safranin-O was higher under visible light. The biochar-ZnO nanocomposite revealed good photocatalytic performance, achieving a Saf degradation efficacy of 83.5% in only 60 min in visible light. The degradation efficiencies of the composite in other environments were estimated to be 81.0% (UV light) and 78% (dark). Similarly, the reduction of MC concentration over time under different conditions is presented in Fig. 11b. The efficiency of MB-ZnO nano- composite was greater in visible light than that of VU and dark conditions. Moreover, the biochar-ZnO nanocomposite exhibited the best photocatalytic performance for MC degradation (56.5%) in only 50 min in visible light. The degradation efficiencies of the composite in other environ- ments were estimated to be 27.5% (UV light) and 25.2% (dark). The degradation of the pollutants in an aqueous solution via MB-ZnO particles can be described according to the already reported mechanism. ZnO is an n-type semi- conductor that has 3.37 eV band gap energy and has absorp- tion ability at room temperature. When photo-induced radiation is equal to or higher than its band gap, an electron (e) is emitted from the valence band and move to the conduc- tion band, creating a positive gap (h+) at the valence band. Thus, this practice creates photogenerated electron-hole pairs (e/h+). Once ZnO particles were illuminated by light with energy higher than the bandgap energy, the conduction-band electrons (e CB) and valence-band holes (h+ VB) were produced on the surface of ZnO particles as presented in (6). Holes could react with water molecules attached to the surfaces of ZnO particles to create highly reactive hydroxyl radicals (OH) as shown in (7). At the same time, oxygen worked as an electron acceptor by producing a superoxide radical anion (O 2) as shown in (8). Pollutant was believed to be broken down via direct oxidation by the OH radicals and O 2 radicals as pre- sented in (9). Previous studies also proved that the electrostatic forces may powerfully affect the removal of pollutants on the biochar-based nanocomposites.

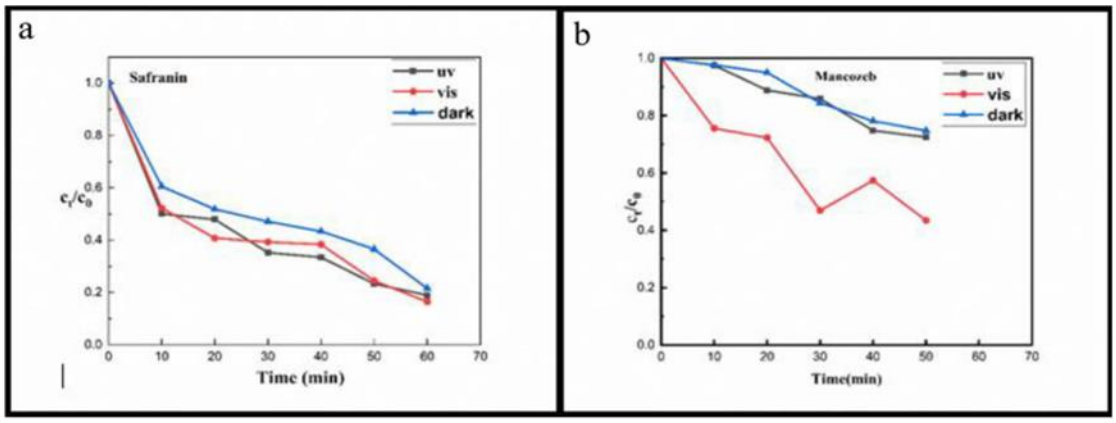


Fig. 11. Efficiency-time degradations of MB-ZnO photocatalyst against Saf (a), and MC (b) in different light sources.

Comparison of photodegradation of pollutants in presence of different light sources

Results of this revealed the optimum catalyst dose (5 mg/100 mL) for the degradation of both Saf and MC pollutants. The degradation of both pollutants was favored at constant pH and temperature. Results of this study also proved MB-ZnO nanocomposite to be a better photocatalyst in all conditions against both pollutants (Fig. 12). The maximum degradation of Saf was observed after 60 min in visible light of 84%. In the case of MC,57 % degradation was noticed in visible light, which is higher than UV and dark in the same duration of 50 mins.

(b).

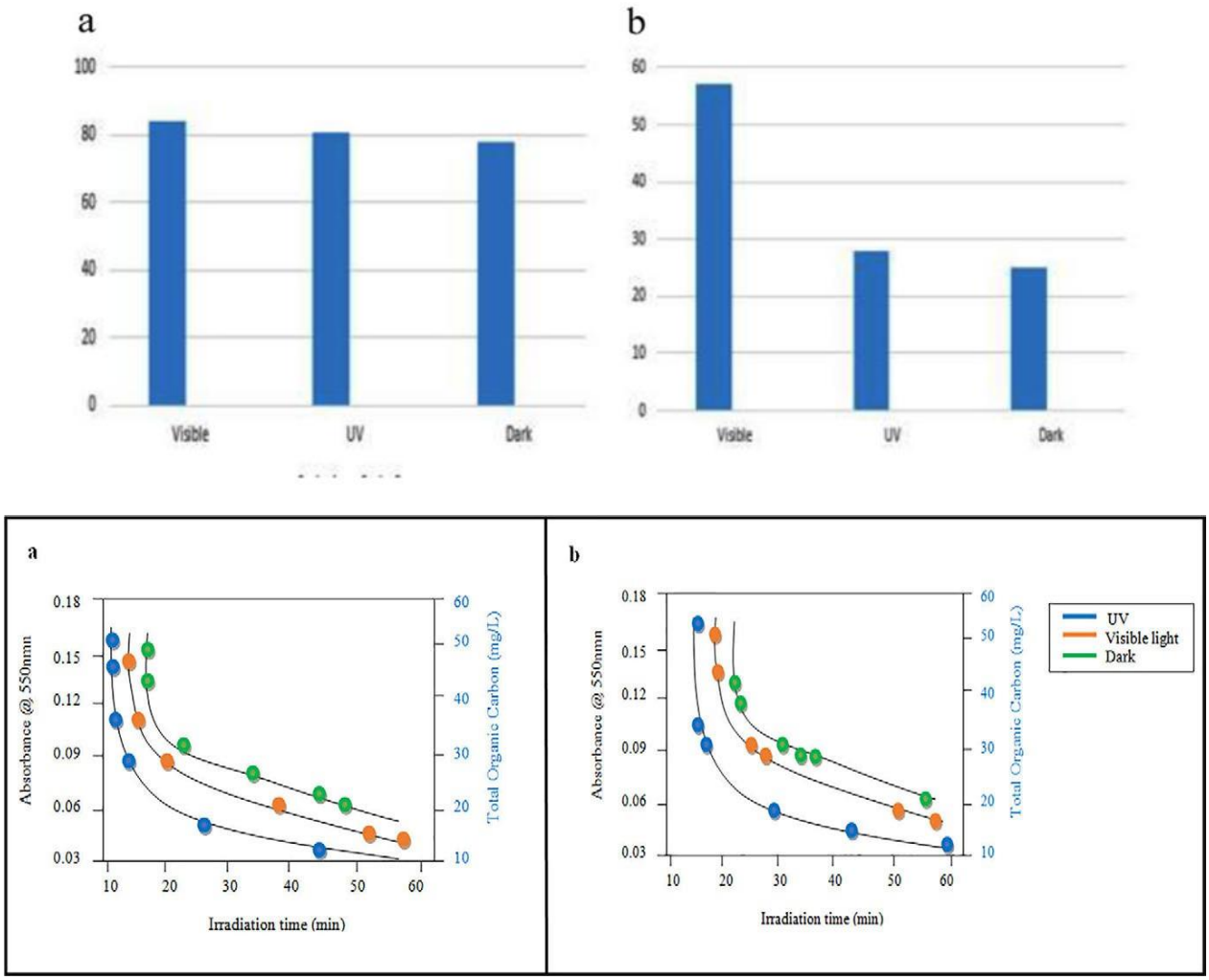


Fig. 12. Degradation efficiency of MB-ZnO nanocomposite in different light sources against Saf (a) and MC

Mineralization of pollutants

For better understanding of the degradation of pollutant under different light sources, TOC was calculated. The decrease in absorption rate with a decrease in TOC concentra- tion was noticed. Reductions in the absorbance peaks indicate the degradation of the Safranin and mancozeb molecules to smaller intermediates (Fig. 13 a, b). All absorption peaks were progressively decreased, and no new absorption peaks appeared during the reaction. Intermediate products formed during the degradation were also successfully degraded towards complete mineralization. Fig. 14.

Reaction kinetics

Plot of TOC removal efficiency vs irradiation time of Saf (a) and MC (b).

Kinetics helps in understanding the mechanisms of pollutant degradation. It is well recognized that the organic pollutants' photo-catalytic degradation follows the Langmuir–Hinshel- wood (L-H) pseudo-first-order kinetic [55] which shows a lin- ear relationship between ln (Co/Ct) and the reaction time. The first-order reaction can be written as:

ln Co=Ct ¼ Kappt 10Þ

For Calculations of reaction kinetics of Saf; Co represents the initial concentration of Saf, t is the reaction time and Ct is the concentration of Saf at reaction time t. So based on the pseudo-first-order equation the activities of the photocata- lyst are calculated by measuring the Saf absorbency in solution was performed at a various time duration under different light sources while containing the same amount of photo-catalyst to determine the solitary influence of the various light sources. It is declared from the results of this study that the removal of the Saf was slight without light (dark) and the photocatalyst had a good effect on the degradation of Saf under the UV and visible light for 60 min (Fig. 13a). The relationship between the apparent reaction

constants (Kapp) for the Saf photo-degradation in the presence of MB- ZnO nanocomposite at 25 °C exposing to different lights is shown in Fig. 13a. From the slopes in Fig. 13a, it can be observed that the apparent rate constant increased significantly for MB- ZnO nanocomposite i.e., 0.93 min1 in dark, 0.94 min1 in UV, and 0.95 min1 in Visible. These results recommend that MB-ZnO nanocomposite performed an efficient and quick pho- tocatalytic degradation of Saf under Visible light. Concluding results indicated that MB-ZnO nanocomposite is one of the best photocatalysts under visible light to remove Saf. The activity of ball-milled MB-ZnO nanocomposite and the influence of various parameters such as dark, UV, and visible light on the kinetics of MC degradation were also studied, suc- cessfully. The MC degradation rate constant was highest (0. 882 min1) in visible, (0.884 min1) in presence of UV, and (0.920 min1) in the presence of dark as shown in Fig. 13b. It can be calculated from the results that BC-ZnO nanocomposite has also indicated an efficient photocatalytic degradation of MC under Visible light.

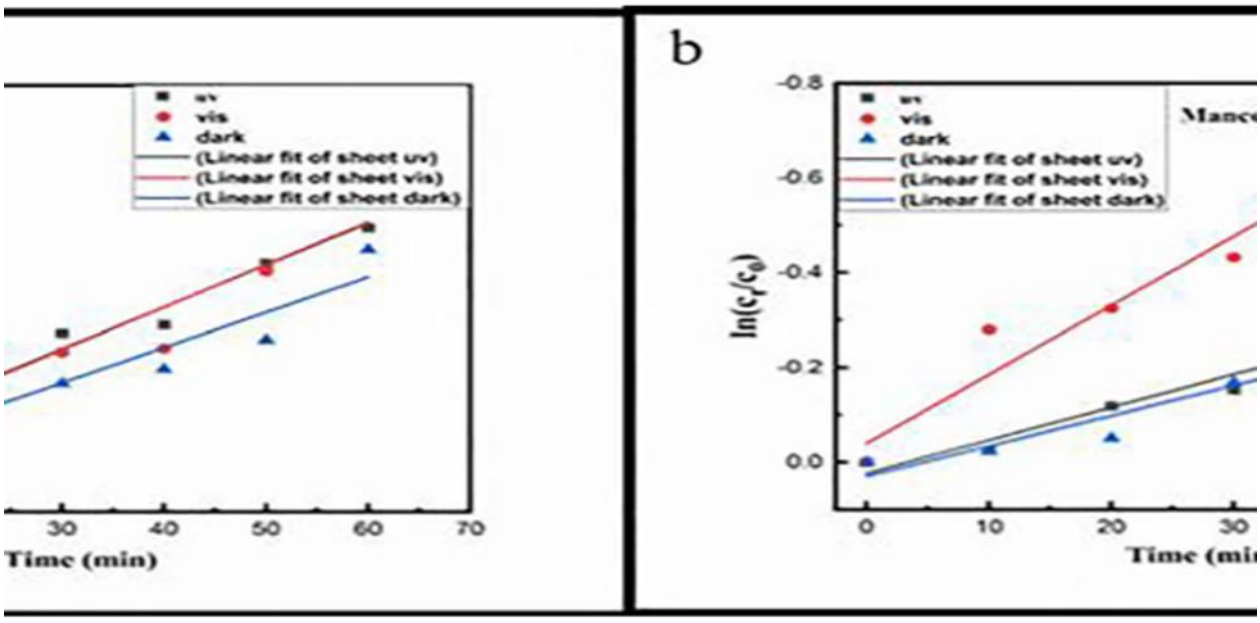


Fig. 14 Plots ln Ct/Co versus time for the absorbance of Saf (a) and MC (b).

Conclusion

Maize-biochar/ZnO nanocomposite was produced by solvent-free ball milling and characterized using complementary structural, compositional, thermal, and optical techniques. Its ability to remove Safranin O and Mancozeb from aqueous solutions was evaluated under dark, UV, and visible-light conditions. Under the reported experimental conditions, the composite removed 83.5% of Safranin O within 60 min under visible light and 56.5% of Mancozeb within 50 min. Removal was lower under UV and dark conditions for Mancozeb, whereas Safranin O also showed substantial removal in the dark, indicating that adsorption may contribute to the observed decrease in concentration. Overall, visible light gave the strongest removal for both pollutants in the reported tests. Further studies should include controls that separate adsorption from photocatalytic degradation, assess catalyst reusability and possible zinc release, and test the material in real wastewater before practical applications are considered.

Ethical statement: Not applicable.

Consent for publication: All authors agreed to publish this work.
Data Availability Statement: Not applicable.
Competing Interest: The authors declare there is no conflict of interest.
Funding: Not applicable.
Clinical trial number: Not applicable.

Author Contributions

Muhammad Rashid Naveed: Conceptualization, methodology, investigation, data collection, and original draft preparation. **Nasreen Ashraf, Samavia Batool:** Formal analysis, data interpretation, and manuscript writing. **Awais Zakeer:** Methodology, validation, technical input, and critical revision of the manuscript. Rabail Urooj: Investigation, literature review, data interpretation, and manuscript editing. **Waqas Ahmad:** Supervision, resources, validation, and critical review of the manuscript. All authors read and approved the final version of the manuscript.

Acknowledgments: We are thankful to all the authors who participated in this work.

References

E. Brillas and C.A. Martínez-Huitle, Applied Catalysis B: Environmental, 166 (2015), 603–643.

X. Xing, W. Li, J. Zhang, H. Wu, Y. Guan and H. Gao, Cellulose, 28(12) (2021), 7953–7968.

S. Singh, N. Singh, V. Kumar, S. Datta, A.B. Wani, D. Singh, K. Singh and J. Singh, Environmental Chemistry Letters, 14(3) (2016), 317–329.

I. Karlsson, H. Friberg, C. Steinberg and P. Persson, PLOS ONE, 9(11) (2014), e111786.

G.M. Patel, J.V. Rohit, R.K. Singhal and S.K. Kailasa, Sensors and Actuators B: Chemical, 206 (2015), 684–691.

A. Anju, S.P. Ravi and S. Bechan, Journal of Water Resource and Protection (2010). Further bibliographic details are not provided in the manuscript.

A. Bhatnagar and M. Sillanpää, Chemical Engineering Journal, 157(2–3) (2010), 277–296.

M. Ramakrishnan and S. Nagarajan, World Applied Sciences Journal, 5 (2009), 114–120.

S.M. de Oliveira Brito, H.M.C. Andrade, L.F. Soares and R.P. de Azevedo, Journal of Hazardous Materials, 174(1–3) (2010), 84 92.

K. Ahmad, H.R. Ghatak and S. Ahuja, Environmental Technology & Innovation (2020), 100893.

Z. Long, Q. Li, T. Wei, G. Zhang and Z. Ren, Journal of Hazardous Materials (2020), 122599.

H. Chen, S.K. Sharma, P.R. Sharma, K. Chi, E. Fung, K. Aubrecht, N. Keroletswe, S. Chigome and B.S. Hsiao, Cellulose, 28(13) (2021), 8611–8628.

M. Tripathi, J.N. Sahu and P. Ganesan, Renewable and Sustainable Energy Reviews, 55 (2016), 467–481.

R. Singh, A. Prakash, B. Balagurumurthy, R. Singh, S. Saran and T. Bhaskar, Journal of Material Cycles and Waste Management, 17(3) (2015), 442–452.

S. Kumar, V.A. Loganathan, R.B. Gupta and M.O. Barnett, Journal of Environmental Management, 92(10) (2011), 2504–2512.

D.D. Sewu, P. Boakye and S.H. Woo, Bioresource Technology, 224 (2017), 206–213.

J. Li, M. Zhang and D. Wang, Bioresource Technology, 263 (2018), 232–241.

W. Li, Q. Dang, C. Robert, D. Laired and M.M. Wright, Bioresource Technology, 241 (2017), 959–968.

J. Shi, J. Wang, L. Liang, Z. Xu, Y. Chen, S. Chen, M. Xu, X. Wang and S. Wang, Journal of Hazardous Materials, 401 (2021), 123382.

M. Kumar, X. Xiong, Z. Wan, Y. Sun, D.C. Tsang, J. Gupta, B. Gao, X. Cao, J. Tang and Y.S. Ok, Bioresource Technology, 312 (2020), 123613.

X. Xu, Y. Zheng, B. Gao and X. Cao, Chemical Engineering Journal, 368 (2019), 564–572.

Y. Zheng, Y. Wan, J. Chen, H. Chen and B. Gao, Chemosphere, 243 (2020), 125344.

C.A. Aggelopoulos, M. Dimitropoulos, A. Govatsi, L. Sygellou, C.D. Tsakiroglou and S.N. Yannopoulos, Applied Catalysis B: Environmental, 205 (2017), 292–301. The volume/year formatting is unclear in the original reference.

L. Damonte, L.M. Zélis, B.M. Soucase and M.H. Fenollosa, Powder Technology, 148(1) (2004), 15–19.

B. Wang, B. Gao and J. Fang, Critical Reviews in Environmental Science and Technology, 47(22) (2017), 2158–2207.

J. Yu, C. Jiang, Q. Guan, P. Ning, J. Gu, Q. Chen, J. Zhang and R. Miao, Chemosphere, 195 (2018), 632–640.

D. Mohan, A. Sarswat, Y.S. Ok and C.U. Pittman Jr., Bioresource Technology, 160 (2014), 191–202.

M. Chen, C. Bao, D. Hu, X. Jin and Q. Huang, Journal of Analytical and Applied Pyrolysis, 139 (2019), 319–332.

M.G. Gonçalves, P.A. da Silva Veiga, M.R. Fornari, P. Peralta-Zamora, A.S. Mangrich and S. Silvestri, Science of the Total Environment, 748 (2020), 141381.

M. Samadi, H.A. Shivaee, A. Pourjavadi and A.Z. Moshfegh, Applied Catalysis A: General, 466 (2013), 153–160.

C. Yang, X. Wang, Y. Ji, T. Ma, F. Zhang, Y. Wang, M. Ci, D. Chen, A. Jiang and W. Wang, NanoImpact, 15 (2019), 100174.

B. Ekka, M.K. Sahu, R.K. Patel and P. Dash, Water Resources and Industry, 22 (2019), 100071.

F. Mohamed, M.R. Abukhadra and M. Shaban, Science of the Total Environment, 640 (2018), 352–363.

F. Yu, Y. Zhou, B. Gao, H. Qiao, Y. Li, E. Wang, L. Pang and C. Bao, Journal of the Taiwan Institute of Chemical Engineers, 67 (2016), 318–324.

H. Sun, O. Zelekew, X. Chen, Y. Guo, D. Kuo, Q. Lu and J. Lin, RSC Advances, 9 (2019), 31828–31833. The original entry also contains an unclear “(1839)” notation.

E. Radich, J. Krenselewski, A.L. Zhu and J. Kamat, Chemistry of Materials, 26 (2014), 4662–4668.

F. Yu, F. Tian, H. Zou, Z. Ye, C. Peng, J. Huang, Y. Zheng, Y. Zhang, Y. Yang and X. Wei, Journal of Hazardous Materials, 415 (2021), 125511.

S. Duo, R. Zhong, Z. Liu, J. Wang, T. Liu, C. Huang and H. Wu, Journal of Physics and Chemistry of Solids, 120 (2018), 20–33.

P. Gholami, L. Dinpazhoh, A. Khataee and Y. Orooji, Ultrasonics Sonochemistry, 55 (2019), 44–56.

N. Batra, M. Tomar and V. Gupta, Analyst, 137(24) (2012), 5854–5859.

T. Arfin and S.N. Rangari, Analytical Methods, 10(3) (2018), 347–358.

M. Pietro and C. Paola, Thermochimica Acta, 413(1–2) (2004), 209–214.

E.Y.L. Teo, L. Muniandy, E.P. Ng, F. Adam, A.R. Mohamed, R. Jose and K.F. Chong, Electrochimica Acta, 192 (2016), 110–119.

Y. Zhang, N. Zhang, Z.R. Tang and Y.J. Xu, ACS Nano, 6(11) (2012), 9777–9789.

Y. Zhang, T.R. Chang, B. Zhou, Y.T. Cui, H. Yan, Z. Liu, F. Schmitt, J. Lee, R. Moore and Y. Chen, Nature Nanotechnology, 9(2) (2014), 111–115.

K.S. Ahn, Y. Yan, S.H. Lee, T. Deutsch, J. Turner, C.E. Tracy, C.L. Perkins and M. Al-Jassim, Journal of The Electrochemical Society, 154(9) (2007), B956.

F. Yu, F. Tian, F. Zou, H. Ye, C. Peng, J. Huang and B. Gao, Journal of Hazardous Materials, 415 (2021), 125511.

Y. Xiao, H. Lyn, J. Tang, K. Wang and H. Sun, Chemical Engineering Journal, 384 (2020), 123311.

J. Huang, A.R. Zimmerman, H. Chen and B. Gao, Environmental Pollution, 258 (2020), 113809.

S. Silvestri, M.G. Gonçalves, P.A. da Silva Veiga, T.T. da Silva Matos, P. Peralta-Zamora and A.S. Mangrich, Journal of Environmental Chemical Engineering, 7(1) (2019), 102879.

K.M. Lee, C.W. Lai, K.S. Ngai and J.C. Juan, Water Research, 88 (2016), 428–448.

R. Saravanan, S. Karthikeyan, V. Gupta, G. Sekaran, V. Narayanan and A. Stephen, Materials Science and Engineering C, 33(1) (2013), 91–98.

J.Y. Choi, K. Heo, K.S. Cho, S.W. Hwang, J. Chung, S. Kim, B.H. Lee and S.Y. Lee, Scientific Reports, 7(1) (2017), 1–8.

A. Zhang, X. Li, J. Xing and G. Xu, Journal of Environmental Chemical Engineering, 8(4) (2020), 104196.

D. Fu, G. Han and C. Meng, Materials Letters, 72 (2012), 53–56.

K. Yari, A. Seidmohammadi, M. Khazaei, A. Bhatnagar and M. Leili, Journal of Environmental Health Science and Engineering, 17(1) (2019), 337–351.

G. Moussavi, H. Hossaini, S.J. Jafari and M. Farokhi, Journal of Photochemistry and Photobiology A: Chemistry, 290 (2014), 86–93.

M.F. El-Berry, S.A. Sadeek, A.M. Abdalla and M.Y. Nassar, Materials Research Bulletin, 133 (2021), 111048.

B.P. Nenavathu, S. Kandula and S. Verma, RSC Advances, 8(35) (2018), 19659–19667.

K. Hayat, M. Gondal, M. Khaled, Z. Yamani and S. Ahmed, Journal of Hazardous Materials, 186(2–3) (2011), 1226–1233.

2026 by the authors; Journal of *Kashmir Journal of Academic Research and Development*. This is an open access article distributed under the terms and conditions of the Creative Commons Attribution (CC-BY) license (http://creativecommons.org/licenses/by/4.0/).